Characterization and hydraulic behaviour of the complex karst of the Kaibab Plateau and Grand Canyon National Park, USA

CASEY J. R. JONES[1], ABRAHAM E. SPRINGER[1]*, BENJAMIN W. TOBIN[2], SARAH J. ZAPPITELLO[2] & NATALIE A. JONES[2]

[1]*School of Earth Sciences and Environmental Sustainability, Northern Arizona University, NAU Box 4099, Flagstaff, AZ 86011, USA*

[2]*Grand Canyon National Park, National Park Service, 1824 South Thompson Street, Flagstaff, AZ, 86001, USA*

**Correspondence: abe.springer@nau.edu*

Abstract: The Kaibab Plateau and Grand Canyon National Park in the USA contain both shallow and deep karst systems, which interact in ways that are not well known, although recent studies have allowed better interpretations of this unique system. Detailed characterization of sinkholes and their distribution on the surface using geographical information system and LiDAR data can be used to relate the infiltration points to the overall hydrogeological system. Flow paths through the deep regional geological structure were delineated using non-toxic fluorescent dyes. The flow characteristics of the coupled aquifer system were evaluated using hydrograph recession curve analysis via discharge data from Roaring Springs, the sole source of the water supply for the Grand Canyon National Park. The interactions between these coupled surface and deep karst systems are complex and challenging to understand. Although the surface karst behaves in much the same way as karst in other similar regions, the deep karst has a base flow recession coefficient an order of magnitude lower than many other karst aquifers throughout the world. Dye trace analysis reveals rapid, conduit-dominated flow that demonstrates fracture connectivity along faults between the surface and deep karst. An understanding of this coupled karst system will better inform aquifer management and research in other complex karst systems.

Characterizing and understanding available water resources is an increasing priority for managers concerned with meeting both ecological and human needs in North America (Salcedo-Sanchez *et al.* 2013) and elsewhere in the world (Bakalowicz 2005; Hua *et al.* 2015; Szocs *et al.* 2015). The patterns of precipitation in the hydrological systems of the western USA are seasonal, with high precipitation in winter (as snowpack) and, in some regions, a strong summer monsoon, which requires significant aquifer storage to meet the requirement for water over extended periods of time. This seasonality of recharge results in a reliance on snowpack and groundwater systems to store water throughout the year, slowly releasing it during drier times. Research has shown that groundwater resources are the dominant control of low (base) flow in surface streams (Liu *et al.* 2008, 2012; Tobin & Schwartz 2012) and that they are essential sources of freshwater. Karst is present in many of these high elevation systems (Weary & Doctor 2014) and research from around the world suggests that high elevation karst aquifers provide an important amount of storage and are crucial to both ecosystems and humans (Han & Liu 2004; Karimi *et al.* 2005; Jemcov 2007; Mueller *et al.* 2017). Karst aquifers supply drinking water to 20–25% of the world's population via groundwater pumping and springs (Kresic & Stevanovic 2010).

High elevation groundwater systems with substantial hydraulic gradients have been found to provide significant groundwater storage and are relatively understudied due to their remote and often inaccessible locations (Clow *et al.* 2003). Karst aquifers in high elevation settings are equally underrepresented in the literature (Tobin & Schwartz 2016). Researchers have shown that these high elevation snow-dominated systems often have rapid conduit development (Faulkner 2009; Lauber *et al.* 2014), substantial amounts of diffuse recharge (Oraseanu & Mather 2000; Perrin *et al.* 2003; Goldscheider *et al.* 2007) and recharge to matrix storage through snowmelt (Tobin & Schwartz 2012). A changing climate may, however, promote more precipitation as rain rather than snowfall, changing the dynamics of snowmelt-dominated karst aquifers worldwide (Gremaud & Goldscheider 2010).

Karst aquifers are known to feed the largest springs in the world, making them essential not only for access to clean drinking and irrigation

From: Parise, M., Gabrovsek, F., Kaufmann, G. & Ravbar, N. (eds) *Advances in Karst Research: Theory, Fieldwork and Applications*. Geological Society, London, Special Publications, **466**, https://doi.org/10.1144/SP466.5

water, but also as habitats for many spring-dependent species (Springer & Stevens 2009; Kresic & Stevanovic 2010) and unique cave-obligate species (Culver & Sket 2000). Groundwater systems provide a mechanism of control for changes in vegetative succession and fluvial geomorphic processes (Batz *et al.* 2016). To better protect these habitats, processes and water supplies, it is crucial to characterize the storage properties of karst aquifers (Scanlon *et al.* 2003).

Roaring Springs, a karst spring, is the sole source of water supplying the Grand Canyon National Park (GRCA) in the southwestern USA. The Redwall–Muav aquifer (R aquifer) of the Kaibab Plateau in the GRCA is part of an extremely complex hydrogeological system. The main aquifer unit is at a substantial depth below the surface of the plateau, with numerous overlying non-karst rock units, complex local and regional structural features, and a perched aquifer, all of which result in intricate recharge flow paths (Huntoon 1970, 1974, 1981; Beus 1990*a*). The Grand Canyon was originally designated as a National Monument in 1908 by President Theodore Roosevelt under the Antiquities Act as 'an object of unusual scientific interest'. The Grand Canyon became a National Park in 1919. Although neither of these descriptions specifically lists karst as one of the reasons for designating the Grand Canyon as an outstanding natural feature, the GRCA is actually the second largest karst region in the US National Park System, exceeded only by the Everglades National Park in Florida (Anderson 2000; Weary & Doctor 2014). Whereas other units of the US National Park System are well known for their karst phenomena, such as Mammoth Cave National Park in Kentucky, the GRCA contains >4000 km^2 of karst features (Weary & Doctor 2014). This includes surficial karst development, major cave development and the deeper R aquifer. Although karst systems are particularly difficult to quantify due to their heterogeneity and anisotropic dynamic nature, part of the GRCA's uniqueness is the depth of the main karst strata: the Redwall and Muav formations are buried >1000 m below the surface (Beus 1990*a*). Above this main aquifer is a smaller-scale limestone and sandstone perched aquifer (the Coconino or C aquifer) and various impermeable confining layers. The C aquifer and other stratigraphic layers affect the R aquifer in distinct ways that have not previously been determined in detail and examining their interconnectedness will lead to an improved understanding of the mechanisms of groundwater flow and storage in a multifaceted system.

The focus of this paper is on the northern rim of the Grand Canyon, located on the Kaibab Plateau in northern Arizona in the southwestern USA (Fig. 1). The karst aquifer in this region supplies numerous large springs that provide desert oasis habitats, drinking water and base flow to the Colorado River (Hart *et al.* 2002). Roaring Springs (Fig. 2) discharges from the R aquifer and supplies potable drinking water for all the residents of the National Park and more than six million yearly visitors to the Grand Canyon. Studies of the R aquifer north of the Grand Canyon, despite its ecological and economic importance, have been localized, resulting in limited datasets and making long-term evaluations challenging. Research in the Grand Canyon is also challenging as a result of difficult access and the extreme climatic conditions, but has enticed scientists for decades. Huntoon (1970, 1974, 1981, 2000) provided a valuable foundation of karst characterization in the Redwall and Muav formations, focusing on structural controls on the Kaibab Plateau, groundwater basin delineation and temporal karst development. Ross (2005), Brown (2011) and Schindel (2015) quantified R aquifer karstification, residence time and geochemical properties, but their analyses were limited by a lack of measurements of high-discharge events and long-term continuous data sampling.

Flow in karst aquifers can be turbulent in conduits and may have three components: intergranular porosity, fractures and conduit-dominated flow (Bonacci & Jelin 1988; Scanlon *et al.* 2003). Karst aquifers are typically challenging to study because of this heterogeneity (Goldscheider *et al.* 2007); in addition, the R aquifer of the GRCA is so deep that conventional methods of determining specific storage and transmissivity are difficult and expensive (Parise *et al.* 2015). However, recent studies and the application of a wider variety of field and geospatial techniques have been applied to better characterize the processes functioning in this karst aquifer system. This paper summarizes these new studies, which have been designed to provide: (1) more detailed characterization of the surficial karst on the Kaibab Plateau using geographical information system and LiDAR analyses; (2) an initial insight into flow paths from the surface to the springs using non-toxic fluorescent dye tracers; and (3) the use of hydrograph recession curves to analyse the recharge response of the R aquifer via Roaring Springs. The unique interactions of the shallow and deep karst systems in the GRCA may be able to better inform aquifer management decisions and research in other karst regions worldwide.

Study area

Located in northern Arizona in the southwestern USA (Fig. 1), the GRCA lies in an area with an arid to semi-arid environment characterized by

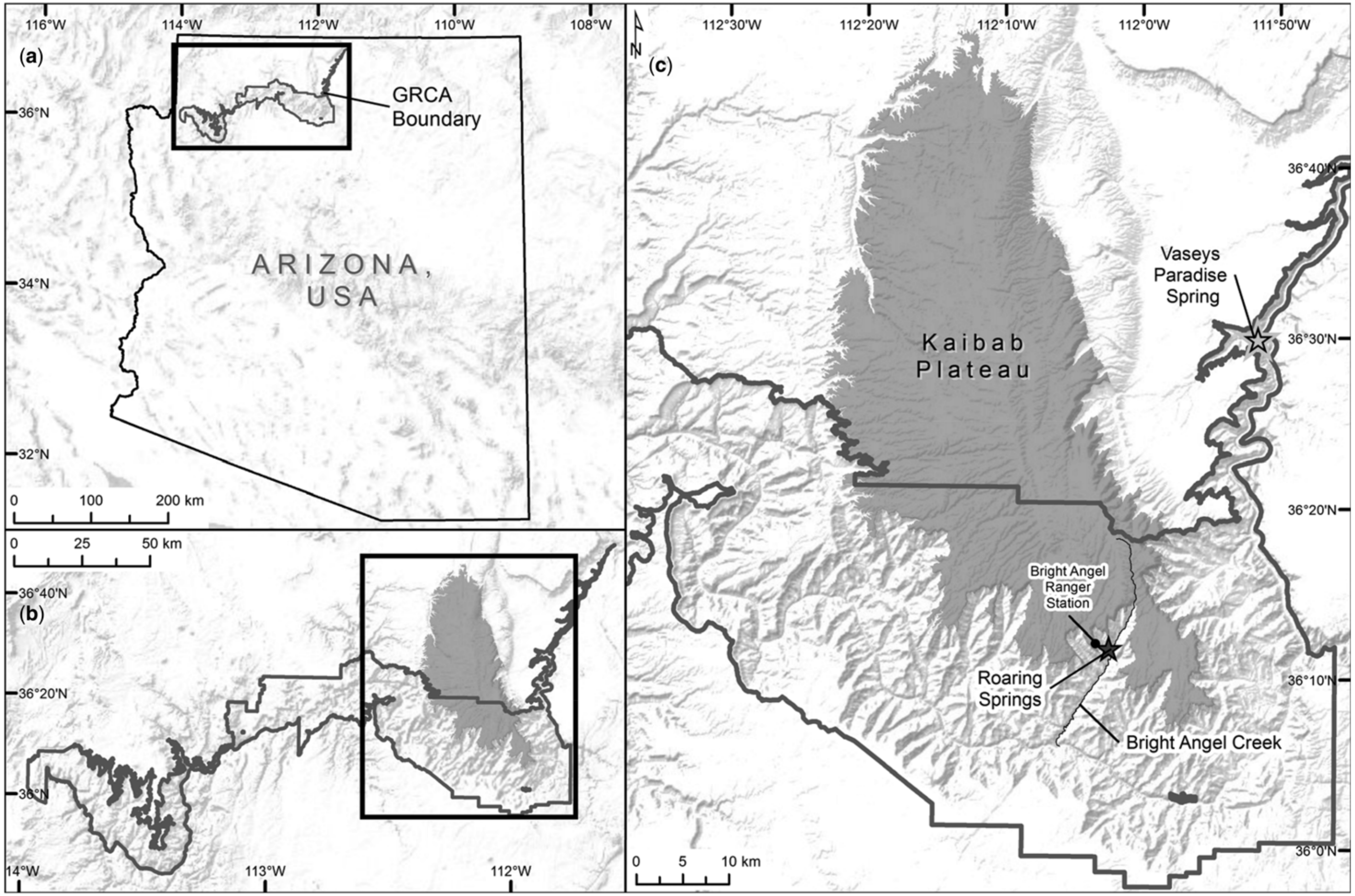

Fig. 1. (**a**) Location map showing the state border of Arizona and the boundary of the Grand Canyon National Park (GRCA). (**b**) Boundary of the GRCA and location of the study area. (**c**) Study area showing the locations of the Kaibab Plateau, the Bright Angel Ranger Station (precipitation data), Roaring Springs, Vaseys Paradise Spring and Bright Angel Creek.

Fig. 2. Photograph of Roaring Springs, Grand Canyon National Park discharging from several outlets (photograph taken by Abe Springer).

extreme vertical relief and stark climate gradients. Bisected by the Colorado River, the sheer canyon walls provide rare access to deep aquifers through springs gushing from caves in the cliff faces. These springs provide potable water, habitats and refuges hundreds of metres below the rim (Figs 2 & 3) in an otherwise desert environment. The Kaibab Plateau is an uplifted region bordered to the south by the North Rim of the Grand Canyon. The region covers *c.* 2460 km^2, existing within the bounds of both the GRCA and the adjoining Kaibab National Forest. Unlike the surrounding arid regions, the Kaibab Plateau is classified as a temperate forest climate, averaging 652 mm of precipitation per year (National Oceanic & Atmospheric Administration 2013) and reaching a maximum elevation of 2810 m a.s.l.

Climate

Precipitation in the Grand Canyon region is typically bimodal, with wet seasons occurring in both the summer and the winter. Winter precipitation is primarily fed by moisture originating in the north Pacific Ocean, which is transported eastward by polar and subtropical jet streams (Sheppard *et al.* 2002; Hereford 2007), whereas the summertime (July–September) precipitation is a result of the North American monsoon (Hereford 2007).

Since 1996, the southwestern USA has been in the midst of what scientists have called the 'early twenty-first century drought' (Cayan *et al.* 2010). Comprehensive climate records exist for the city of Flagstaff, Arizona, 130 km south of the Grand

Fig. 3. Photograph of Vaseys Paradise Spring, Grand Canyon National Park (photograph taken by Abe Springer).

Canyon. A 30% reduction in accumulated precipitation was observed in Flagstaff between 1996 and 2011 compared with the preceding 15 years (1981–96) (Hereford 2007). This reduction occurred mostly in winter precipitation, which is substantially influenced by large oceanic–atmospheric cycles that affect the winter temperatures and precipitation in the southwestern USA. The El Niño Southern Oscillation and the Pacific Decadal Oscillation (PDO) have been shown to affect weather patterns (Sheppard *et al.* 2002). Warm PDO phases have coincided with increased moisture in the southwestern USA, whereas cool phases in the PDO have coincided with drier conditions. The current 'early twenty-first century drought' in the SW has coincided with the latest cool phase of the PDO beginning in 1999 (Sheppard *et al.* 2002; Hereford 2007).

Recharge area, sources and mechanisms

The Kaibab Plateau is a classic representation of a snowmelt-dominated karst aquifer system. Snowmelt runoff and precipitation infiltrate the Kaibab Plateau rapidly via sinkholes, faults and fractures, and slowly through diffuse infiltration. Once in the subsurface, it travels hundreds of metres vertically and kilometres laterally through the karst system in the R aquifer (Brown 2011). Most precipitation (*c.* 60%) falls during the winter (November–March) as snow, which subsequently melts during spring (March–May) when low temperatures, minimal plant use and saturated conditions in the vadose zone allow more water to recharge the aquifer system. Roaring Springs primarily responds to recharge as a result of melting of the winter snowpack, with relatively little recharge to base flow occurring during the summer monsoon season (Ross 2005; Schindel 2015). Discharge from winter snowmelt peaks during late spring and decreases to base flow fed by the primary intergranular porosity during the summer monsoon season (Ross 2005) (Fig. 4).

Stratigraphy

The stratigraphy in the Grand Canyon is globally renowned and well-studied due to tremendous exposures resulting from a combination of the Kaibab Plateau uplift and downcutting by the Colorado River. Numerous studies have focused on quantifying the different stratigraphic layers and evolutionary

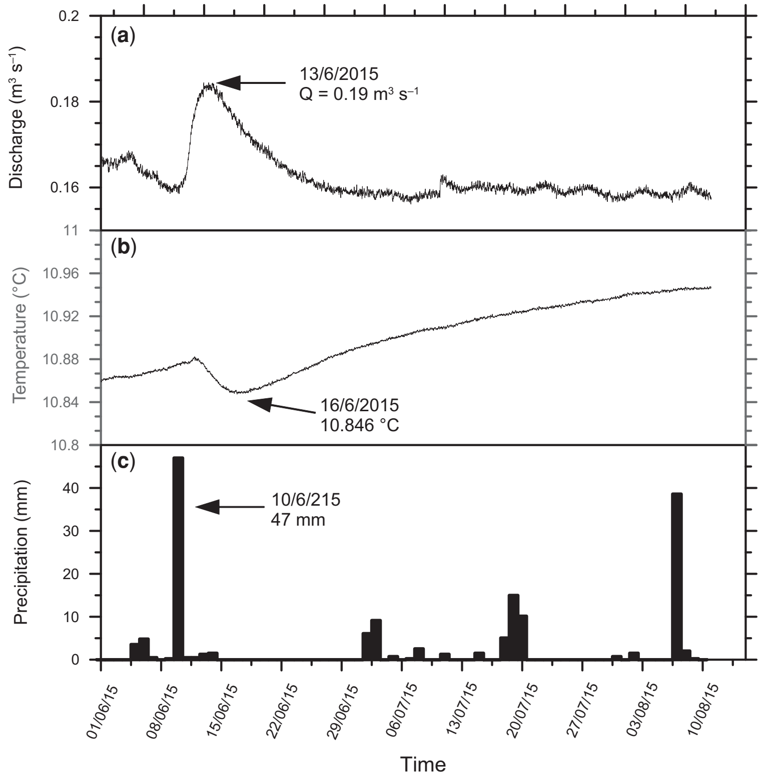

Fig. 4. (**a**) Discharge and (**b**) temperature response at Roaring Springs following a (**c**) 47 mm monsoonal precipitation event on 10 June 2015 over the Kaibab Plateau that drained to the spring.

history of the Kaibab Plateau over multiple decades (Huntoon 1974; Beus 1990*a*). The deep canyon and the regional, southward-dipping strata create two distinct aquifers with very different recharge areas and flow paths. Although more studies have focused on the aquifers of the southern rim of the canyon due to ease of access and the regional dependence on groundwater (Crossey *et al.* 2006), the aquifers of the Kaibab Plateau on the North Rim are less affected by human development and thus are less studied. Although the karstic R and C aquifers are the focus of this paper, the overlying and underlying units of the R and C aquifers are relevant for a comprehensive understanding of the hydrogeology (Fig. 5).

The R and C aquifers occur within Paleozoic strata of the canyon. Underlying this is a crystalline, Precambrian core and the sedimentary Grand Canyon Supergroup. These strata typically have very low porosity with minimal water storage. The Paleozoic sequence consists of sedimentary rocks, including sandstone, limestone and shale (Fig. 5). The Bright Angel Shale, a *c.* 100 m thick layer in this part of the Grand Canyon, acts as a regional aquitard, causing nearly all the groundwater to discharge at or above the shale (Huntoon 1974; Ross 2005). The composition of micaceous clay seals any secondary faulting or fracturing, further reducing the Bright Angel Shale's permeability (Huntoon 1974).

Overlying the Bright Angel Shale are strata that compose the R aquifer: the Muav, Temple Butte and Redwall formations (Fig. 5). These lower Paleozoic carbonates are well recognized in the Grand Canyon as steep, vertical cliffs and have low primary porosity unless fractured or karstified (Huntoon 1974). However, the large amount of dissolution and faulting in this aquifer causes it to be one of the largest stores of groundwater in this region.

The oldest layer in the R aquifer is the Muav Formation, a *c.* 100 m thick layer composed of laminated carbonates along with dolomitic and calcareous mudstone (Middleton & Elliot 1990) (Fig. 5). A complex intertonguing relationship characterizes the contact between the Muav Formation and the Bright Angel Shale. The Muav Formation is the base of the R aquifer and the majority of large springs below the Kaibab Plateau emerge at the contact between the Muav Formation and the Bright Angel Shale. Overlying the Muav Formation is the

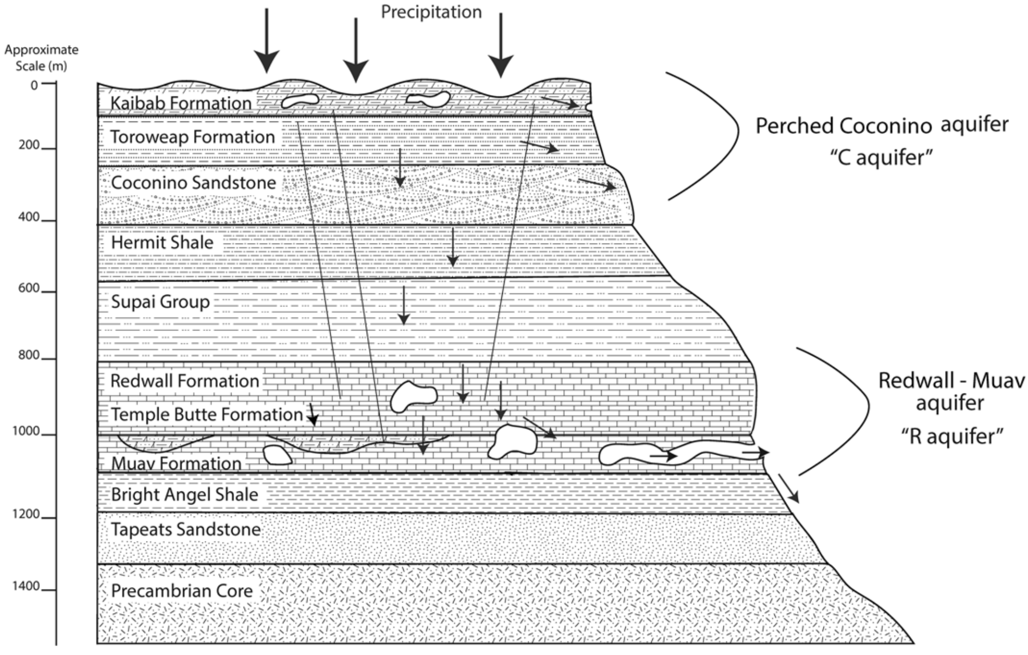

Fig. 5. Idealized conceptual profile oriented along the plane of a permeable fault zone cross-cutting all the strata and serving as a vertical hydraulic conduit. The permeable fault zone vertically connects an aerially extensive circulation system within the C aquifer. This circulation system drains to the fault and to horizontal karst conduits dissolved along the plane of the fault within the R aquifer.

Temple Butte Formation, which consists of dolostone lenses, most often <30 m thick (Beus 1990*b*). The Temple Butte Formation is negligible in the Kaibab Plateau region. The overlying Redwall Formation forms stark red cliffs stained by iron oxide from the overlying Supai Group. The Redwall is up to 250 m thick and consists predominantly of limestone (Beus 1990*a*). Large cavern development occurs throughout this formation (Huntoon 2000). Although there are a few hydrologically active unconfined caves, the Redwall Formation is primarily home to the majority of hydrologically inactive caves in the GRCA. Karstification throughout the formation has occurred along fractures parallel and sub-parallel to regional faults and fractures (Hill & Polyak 2010).

Huntoon (1974) has suggested that these caves and associated groundwater movement were driven by existing geological structures, with flow occurring along faults and fractures. Subsequently, Huntoon (2000) proposed that the dewatering of the aquifer and movement of springs from the Redwall Formation to the stratigraphically lower Muav Formation was due to the incision of the Grand Canyon and associated tributaries, such as Bright Angel Creek. The dissolution that forms the currently active karst springs and hydrologically inactive caves has been the result of a combination of epigenic and hypogenic waters, creating a unique karst system (Hill & Polyak 2010).

Between the R aquifer and the perched C aquifer are >300 m of sedimentary rock that act as a leaky aquitard. Although these formations are not water-bearing, they are important in the transport of water from the surface and the C aquifer to the R aquifer below. The Supai Group (Wescogame, Watahomigi and Manakacha formations and the Esplanade Sandstone) and the Hermit Shale compose the stratigraphic units between the R and C aquifers. The complex Supai Group is primarily composed of sandstone, mudstone and some limestone and dolomite, whereas the Hermit Shale consists of siltstones and mudstones (Blakey 1990). The rocks of these stratigraphic units have low permeability where undisturbed, but groundwater flows along localized faulting, vertical joints and bedding partings (Huntoon 1970).

The C aquifer occurs within the uppermost portion of the Grand Canyon stratigraphic sequence and consists of the Coconino Sandstone, the Toroweap Formation and the Kaibab Formation (Fig. 5). The C aquifer is a minor water-bearing unit, but small-scale springs do discharge on and near the North Rim and around the perimeter of the Kaibab Plateau (Huntoon 1970; Ross 2005). Where the underlying Hermit Shale is undisturbed, the C aquifer appears to have greater saturation and behaves as a perched aquifer. The Coconino Sandstone is *c.* 100 m thick and is a fine- to medium-grained cross-bedded quartz sandstone (Ross 2005). Overlying the Coconino Sandstone is the Toroweap Formation, which includes *c.* 120 m of non-cross-bedded sandstone, gypsum and limestone. The Kaibab Formation occurs at the surface of the Kaibab Plateau and is highly variable in thickness due to erosion. The formation is largely composed of gypsum, dolostone, chert and limestone (Huntoon 1970; Hopkins 1990). The Kaibab Formation is highly karstified with substantial dissolution along faults and fractures. The gypsum in the underlying Toroweap Formation is also highly susceptible to dissolution. The combination of karst features in the Toroweap and Kaibab formations has created an abundance of closed depressions throughout the region (Huntoon 1970).

Surface karst system

The near-surface karst system in the Kaibab and Toroweap formations of the C aquifer on the Kaibab Plateau is a defining feature of the plateau and the sinkholes provide the primary means of recharge to the underlying aquifers (Huntoon 1974, 2000). The unconfined nature of both the C and R aquifers on the plateau results in aquifer responses to storm events that are commonly flashy and variable, depending on the precipitation and the season (Huntoon 2000). These sinkholes recharge an underlying conduit system, both of which are structurally controlled. Limited geophysical evidence is available to map these conduits; however, the morphology of the sinkholes above these conduits can be indicative of conduit size and the ability to channel, store and discharge the incoming water (Panno *et al.* 2013). Geographical information system and LiDAR data for sinkholes were used to better quantify the surficial properties of the C aquifer and to relate the sinkholes as infiltration points to the overall hydrogeology of the system.

Surface karst methods

A sinkhole layer was created from 1 m resolution LiDAR data to characterize the sinkholes of the Kaibab Plateau (Fig. 6). Watershed Sciences was contracted by 3DiWest to fly LiDAR over the Kaibab Plateau for the Kaibab National Forest, Kaibab Ranger District to assess the habitat of the raptor species the northern goshawk. Ground returns with a resolution of 1 m were acquired. The elevation data were masked to an elevation of 2292 m and above to isolate the plateau surface. Depressions were delineated using a basin-fill function in ArcGIS 10.2 (ESRI 2014). The basin-fills were subtracted from the original topographic LiDAR data to create a depression layer. To reduce noise, this layer was smoothed using two iterations of the Focal Statistics-Mean function in ArcGIS (ESRI 2014) set to a 3 × 3 smoothing parameter. This smoothed layer was reclassified and filtered, resulting in sinkholes with a minimum depth of 0.1 m. The sinkhole size statistics table was then exported into Python Programming Language and filtered to eliminate all sinkholes smaller than four pixels in area (4 m^2) to remove artefacts and anthropogenic depressions (Fig. 7). A small sample of field observations and measurements was used to inform the parameters chosen to filter our model. However, additional field measurements would add value to, and increase the accuracy of, these parameters in future studies because field measurements remain a key component of sinkhole investigation to verify topographic data (Basso *et al.* 2013). Python Version 2.7.12 (Pyton Software Foundation 2016) was used to calculate the measures of sinkhole development, including the depression density and sinkhole area ratio (White 1988), in addition to general sinkhole population size statistics.

To assess similarities between the Kaibab Plateau sinkholes and other karst areas around the globe, sinkhole distributions were grouped by depth and plotted as a frequency–depth distribution using the equation:

$$n = N_o e^{-kd} \tag{1}$$

where n is the number of sinkholes with a certain depth group, N_o is a constant representing the total number of sinkholes, k is a constant corresponding to the rate of attenuation of the number of sinkholes per depth and d is the depth of the sinkhole (Troester *et al.* 1984).

Surface karst results

The sinkhole analysis method delineated a total of 7457 sinkholes over the 1.45×10^3 m^2 area of the Kaibab Plateau, with volumes ranging from 0.40 m^3 to >1.4×10^6 m^3 (Table 1). The majority of the sinkholes were at the smaller end of the spectrum, typical of most surface karst (White 1988). A linear relationship ($r^2 = 0.68$) between the two-dimensional area of a sinkhole and its depth exists on the Kaibab Plateau (Fig. 8). A map of sinkhole density on the Kaibab Plateau is shown overlain by the mapped geological structures and reveals a correlation between sinkhole density and the presence of faults and fractures (Fig. 9).

A comparison of sinkhole frequency–depth distributions between the Kaibab Plateau and other karst regions shows that the Kaibab Plateau

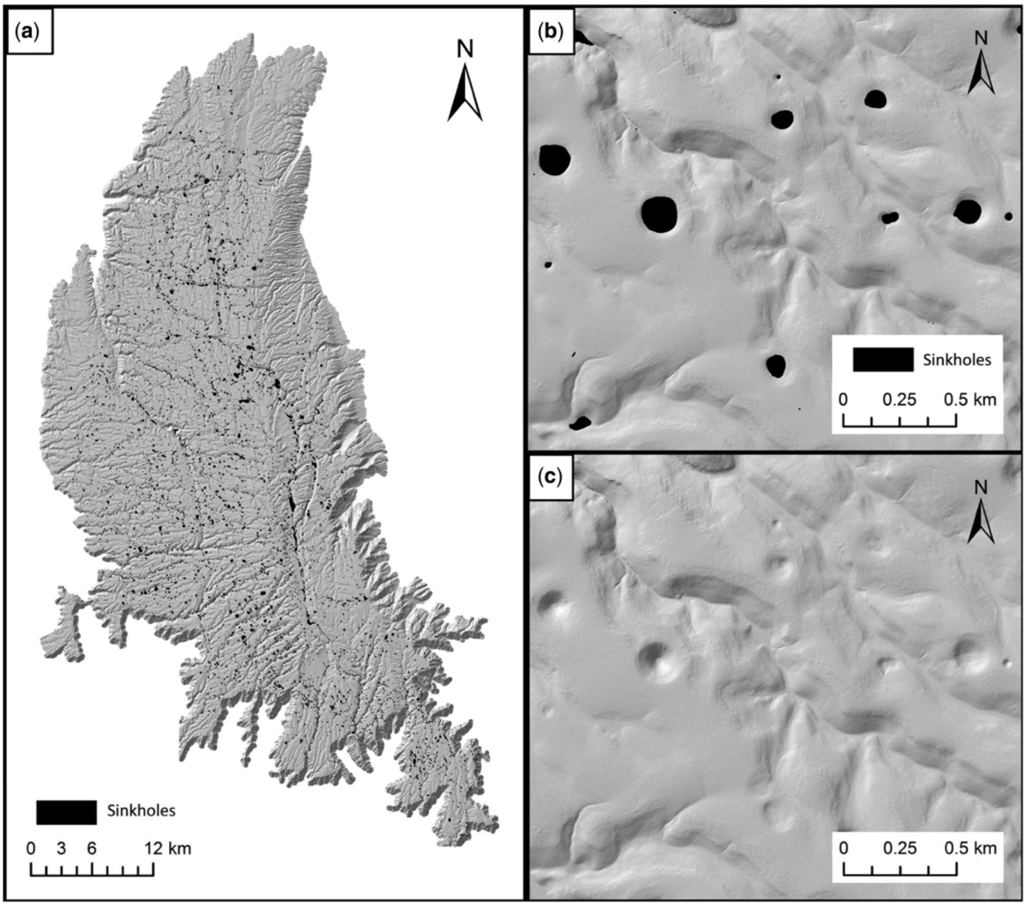

Fig. 6. (**a**) Hillshade layer of LiDAR elevation data of the Kaibab Plateau overlain with ArcGIS-automated sinkholes in black. (**b**) An enlarged section of the Kaibab Plateau LiDAR with Arc-GIS-automated sinkholes in black. (**c**) The same enlarged section of the Kaibab Plateau with the sinkhole layer removed.

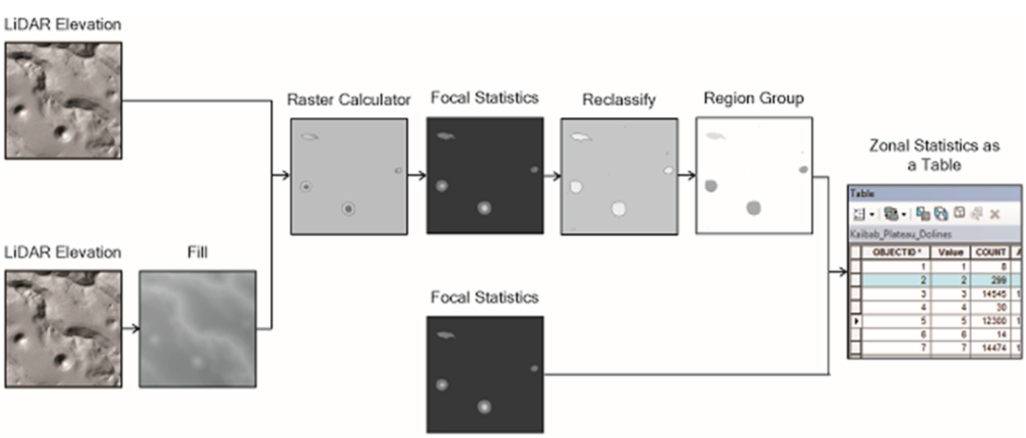

Fig. 7. Flow chart of ArcGIS functions used to identify sinkholes on the Kaibab Plateau and their measurements of area, depth and volume.

Table 1. *Statistical measurements for the Kaibab Plateau sinkholes*

	Depth (m)	Area (m^2)	Volume (m^3)
Minimum	0.10*	4*	0.40
Maximum	48.8	3.76×10^5	1.42×10^6
Mean	1.14	1.32×10^3	4.62×10^3

*Controlled value.

sinkhole depth distribution has a trend line equation of $n = 7460e^{-25d}$, which, when normalized, falls close to the trend line equation for the sinkhole plain of south-central Kentucky (Fig. 10, Table 2).

Surface karst discussion

The majority of the sinkholes were on the smaller end of the spectrum, typical of most surface karst (Table 1, Fig. 8; White 1988). Sinkholes plotted above the trend line in Figure 8 are likely to be steeper and more erosive, indicative of a larger conduit system capable of channelling, storing and discharging larger amounts of water. Sinkholes below the trend line are more likely to be shallow and wide, and may be closely tied to portions of the conduit system that have a lower drainage capacity. These characteristics could prove valuable in future vulnerability mapping of the Kaibab Plateau (Panno *et al.* 2013).

Figure 9 also illuminates a relationship between sinkholes and the location of possible active conduits near regions of major faults and fractures. A similar density model reported by Panno *et al.* (2008) suggests that sinkhole densities are higher in areas with prominent conduit systems. This interpretation is consistent with the conduit hypotheses developed by Huntoon (1974, 2000): dominant conduits exist in the proximity of faults and fractures on the plateau. Such conduits in highly fractured and faulted areas are hypothesized to provide direct connections between the surface and the shallow and deep karst systems of the plateau. Future investigations of sinkhole circularity and azimuth in relation to faults, fractures and joints would help to clarify the presence of structurally driven sinkhole formation on the Kaibab Plateau (Brinkmann *et al.* 2008; Basso *et al.* 2013).

The frequency–depth distribution trend line for the Kaibab Plateau is similar to the trend line of the sinkhole plain of south-central Kentucky (Fig. 10, Table 2) (Troester *et al.* 1984). The size and density characteristics may indicate that the overall geomorphology of the karst conduit system on the

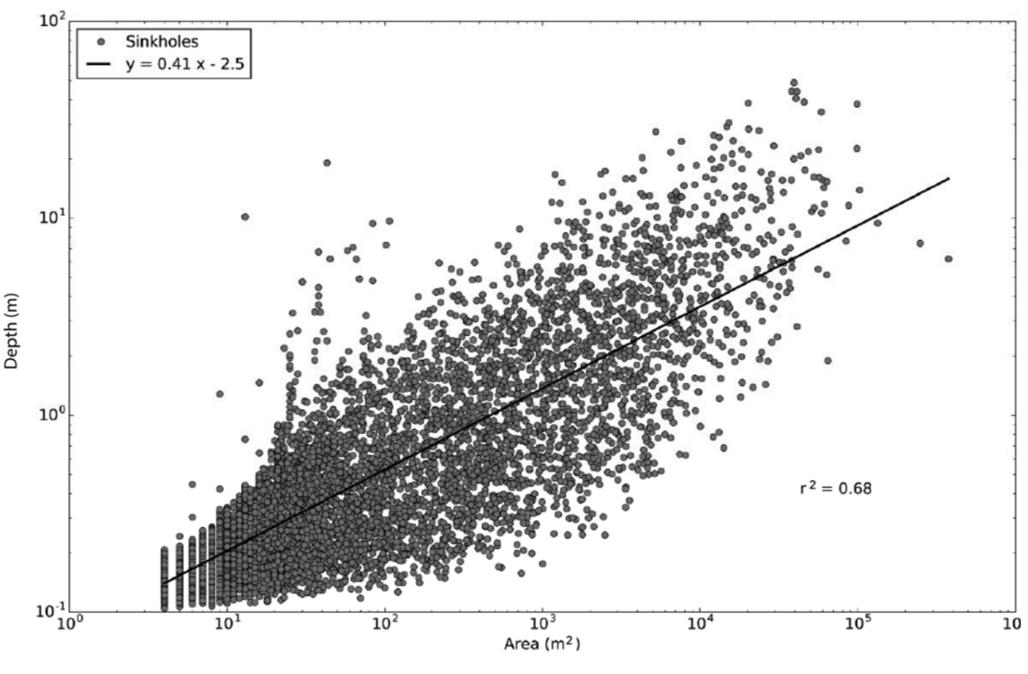

Fig. 8. Scatterplot of the positive relationship between the depth and area of sinkholes on the Kaibab Plateau. Note that both axes are on a logarithmic scale.

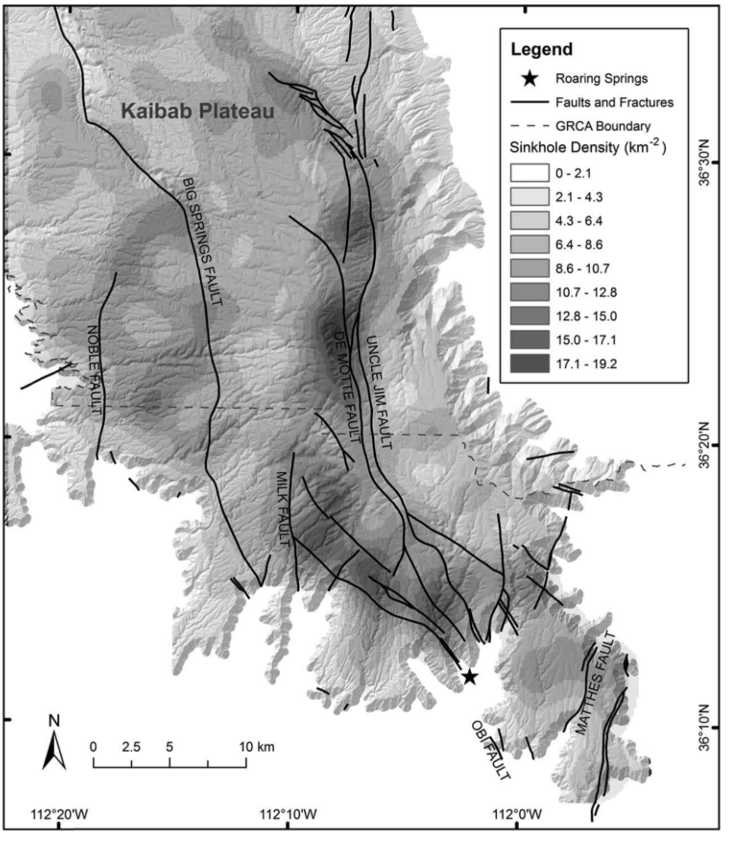

Fig. 9. Map of the Kaibab Plateau showing the density of sinkholes per km^2 overlain with known faults and fractures in the region. Note that the sinkhole density increases with proximity to faults.

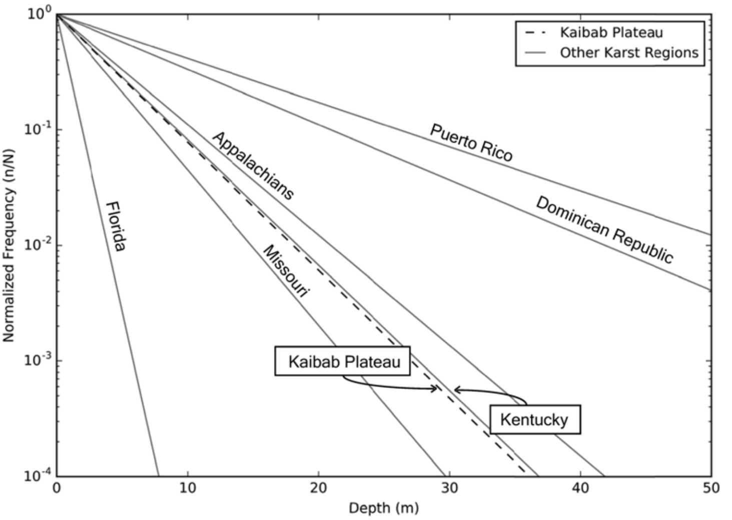

Fig. 10. Graph of the frequency–depth distribution exponential decay trend lines fitted to the karst regions in Troester *et al.* (1984) compared with those for the Kaibab Plateau sinkholes. Note that the slope of the Kaibab Plateau and the Kentucky trend lines are almost identical, indicating similar karst behaviour.

Table 2. *Properties of sinkhole populations and least-squares fitting coefficients for exponential depth distribution from equation (1)*

Karst region	Total number of sinkholes	Depression density (km^{-2})	Mean depth (m)	$D^e = 1/k$ (m)	N_o	k (m^{-1})	r^2
Temperate karst regions							
Appalachian mountains	5.16×10^3	1.25	7.8	4.48	1.26×10^4	0.22	0.99
Kentucky	8.30×10^2	5.41	5.4	4.02	8.92×10^2	0.25	0.99
Missouri	2.22×10^3	–	6.8	3.23	9.79×10^3	0.31	0.99
Florida	3.40×10^3	7.94	–	0.85	1.23×10^4	1.18	0.99
Kaibab Plateau	7.46×10^3	5.14	1.14	3.95	7.46×10^3	0.25	0.76
Tropical karst regions							
Puerto Rico	4.31×10^3	5.39	19	11.35	6.88×10^3	8.8×10^{-2}	0.99
Dominican Republic	7.21×10^3	5.71	23	8.93	6.92×10^4	0.11	0.99

N_o is a constant representing the total number of sinkholes, k is a constant corresponding to the rate of attenuation of the number of sinkholes per depth and r^2 is the fit of the modelled equation (1) to the actual sinkhole depth–frequency distribution (table adapted from Troester *et al.* 1984).

Kaibab Plateau is similar to that of temperate karst regions. The overall groundwater distribution patterns may follow similar trends, at least within the upper 90–100 m of the Kaibab Formation.

Deep karst system

The deep, karstic R aquifer of the Kaibab Plateau cannot be properly understood without acknowledging the interplay and dependence between it and the shallower components of this karst system. The R aquifer of the Kaibab Plateau is buried beneath a thick series of Paleozoic rocks and only outcrops to the east, west and south of the plateau, where it is bounded by deeply incised canyons. There are springs throughout the outcropping of the aquifer, indicating that recharge is probably not occurring in these locations. This suggests that all the water recharging the aquifer is via sinkholes in the overlying rocks. Recharge to the deep aquifer moves first through the perched karstic C aquifer. Groundwater then continues through non-karstic strata between the C aquifer and R aquifer via faults, joints and bedding partings, all of which alter the groundwater flow dynamics of the R aquifer. The interconnection between the two karst aquifers was interpreted through a dye tracer study and hydrograph analysis of discharge from the deep aquifer.

Dye tracer study

A qualitative tracer study was initiated in 2015 to determine the interconnection between sinkholes on the Kaibab Plateau and springs discharging from the R aquifer. This was the first dye trace study conducted in the region.

Dye injection methods. Four different non-toxic fluorescent dyes were injected into four different sinkholes over a two-year period (Fig. 11) to target those sinkholes whose recharge was theorized, based on research by Huntoon (1974), to contribute to Roaring Springs. The amount of dye was determined following the methodology of Worthington & Smart (2003). The injections were made just after snowmelt at two sinkholes in the GRCA in 2015 and just prior to snowmelt at two sinkholes adjacent to the GRCA in 2016 (Fig. 11). On 21–22 April 2015, 1.5 kg of phloxene B and 1.5 kg of sulforhodamine B dyes were flushed into the sinkholes using 3028 l of water each from water trucks, due to lack of flowing water at the time of injection. This lack of flowing water and the finite amount of water used for the injection probably resulted in the dyes being stranded in the shallow subsurface and they were not detected in the deep flow system.

As a result of the lack of positive results, access limitations, weather uncertainty and the remote nature of all the sites, it was not possible to conduct the 2016 injection during snowmelt. Instead, on 22 February 2016, 3 kg of eosin and 5 kg of uranine were buried in the snow within the sinkholes just prior to snowmelt and the subsequent snowmelt flushed the dyes into the groundwater system (Fig. 11). This method is not ideal because it increases the risk of exposing the dyes to increased photolytic decay and also increases the uncertainty of the flow rates, but it has the advantage of ensuring that there is enough water to push the tracer through the aquifer (Benischke *et al.* 2007). Flowing water generally only exists on the Kaibab Plateau during snowmelt, which is typically rapid, occurring over the course of days to weeks.

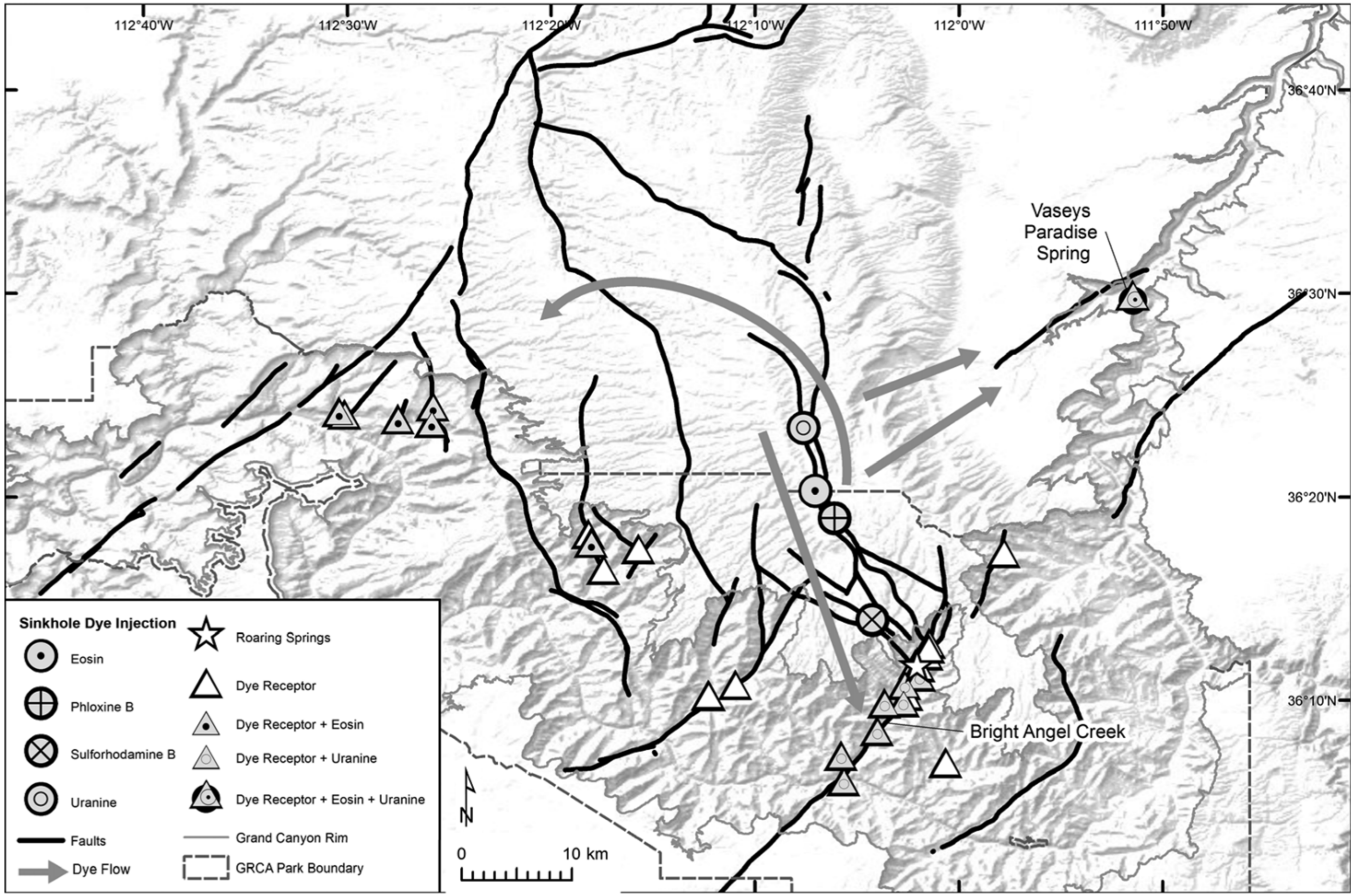

Fig. 11. Locations of the four dye injection sites and the 29 dye receptor sites. Phloxene B and sulforhodamine B were injected during April 2015; eosin and uranine were injected during February 2016. Eosin and uranine (filled triangles) were detected between February and July 2016. The potential generalized flow paths of the eosin and uranine dyes along faults are superimposed on the map. Phloxene B and sulforhodamine B had not been detected by July 2016.

Dye receptor methods. Passive dye monitoring occurred at 29 locations throughout the GRCA (Fig. 11). These monitoring locations were distributed to capture the discharge from more than 41 perennial springs; some locations were in creeks fed by multiple springs. Most of the springs were located at the base of the Muav Formation, with two occurring in the Redwall Formation. Although this methodology limits the amount of data it is possible to collect on the more detailed characteristics of the aquifer (Benischke *et al.* 2007), it was chosen due to a lack of background knowledge of the flow paths, the large number of springs potentially connected to recharge features on the Kaibab Plateau, and the difficulty in accessing and maintaining the monitoring sites.

The dye receptors consisted of nylon mesh packets containing activated charcoal and were assembled at the GRCA physical science laboratory following established protocols (Schindel *et al.* 2007). The receptors were collected and replaced at irregular intervals as allowed by the field conditions and the availability of personnel. Receptor placement and handling procedures were established to maximize the likelihood of recovering the dyes and to minimize the potential sources of error and cross-contamination of samples. After field collection, the dye receptors were rinsed, dried and shipped for analysis. The prepared receptors were analysed by Karst Works (San Antonio, TX, USA) following established methods (Schindel *et al.* 2007). The dyes used for the tracer test and other potential fluorescent substances in the system (from fire retardants and the water infrastructure) were analysed by the laboratory to verify their presence or absence in the receptors.

Methods of dye tracer spatial analysis. We assessed the relationships between positive dye locations, the regionally mapped geology and previous assumptions of flow paths using ArcGIS 10.2 (ESRI 2014) to determine the likely flow paths of the recovered dyes. The results from the dye tracer study were directly overlain on the assumed groundwater basins and flow paths using geological mapping data from Huntoon (1974). The assumed pathways were then modified based on the tracer results.

Results of dye tracer study. Based on the theoretical flow paths from Huntoon (1974), it was assumed that all of the injected dyes would discharge to Roaring Springs or to adjacent springs in Bright Angel Creek. However, eosin, the first dye detected, discharged at springs to the west and one to the east at Vaseys Paradise Spring, but not south near Bright Angel Creek as anticipated (Fig. 11). Eosin was detected between February and May 2016, with the initial detection occurring less than one month after injection. The dye persisted in the system for an additional two months before it was no longer detected (Table 3).

Uranine was detected between May and July 2016. The dye was detected in tributaries to Bright Angel Creek downstream of Roaring Springs and also to the east at Vaseys Paradise Spring (Fig. 11). Uranine injected in February 2016 arrived at these sites within three months of injection and was detected for an additional two months after the initial detection. The other two dyes injected in April 2015 were not detected at any of the dye receptor sites by July 2016.

Discussion of dye tracer study. When the surficial locations of the major faults are overlain on the dye detection results from the eosin test, the patterns that emerge can be related to the flow directions along faults described by Huntoon (1974). Karst is well known for complicated and, at times, unexpected conduit flow paths, and the fault-related structures on the Kaibab Plateau could be avenues for major conduit flow through the plateau. This interpretation may or may not be that simple when we

Table 3. *Dye tracer results for eosin and uranine injections*

Injection site	Injection elevation (m)	Amount of dye (kg)	Recovery site	Recovery elevation (m)	Distance between injection and recovery (km)	First detection after injection (months)
Eosin	2687	3	Deer Spring	835	35	<1
			Thunder River	980	31	<1
			Tapeats Spring	1125	28	<1
			Vaseys Paradise	895	29	<1
			Merlin Spring	1355	17	<1
Uranine	2657	5	Transept Creek	1300	24	2–3
			Ribbon Creek	1255	26	2–3
			Phantom Creek	940	30	2–3
			Wall Creek	1180	26	2–3
			Vaseys Paradise	895	27	2–3

consider the propagation of the surface expression of these faults through the various layers of limestone, sandstone and shale (Fig. 5). Shale typically deforms plastically along faults and therefore is considered to be a barrier to flow. Potential conduit flow along faults indicates that either the faulted shale is not acting as a barrier to flow, or that the flow could be predominantly along parallel and sub-parallel fractures related to the faults. Huntoon (1974) noted that the caves generally follow major fractures sub-parallel to larger regional faults. It is likely that more water follows these sub-parallel fractures than the faults themselves as a result of the prohibition of flow by deformation along the faults. In addition, because cave passage patterns in the region show strong fracture control (Fig. 12) highly related to the faults and fractures mapped on the surface, similar patterns may exist in intermediate geological units.

The results of the eosin dye tracer study suggest that the flow patterns follow the hypotheses proposed by Huntoon (1974); however, the locations of the detection of the uranine dye complicate these interpretations. The uranine dye was injected into the northernmost of two sinkholes associated with the same fault, whereas the eosin dye was injected into the southernmost of the two sinkholes. Although the eosin dye arrived at springs east and west, but not south, of Bright Angel Creek (Fig. 11), the uranine dye discharged into the tributaries feeding the creek south of Roaring Springs as well as to the east at Vaseys Paradise Spring. The contradictory arrival of uranine in Bright Angel Creek to the south suggests two possible explanations: (1) differences in horizontal and vertical flow paths from each sinkhole or (2) differences in the types, sources and timing of the water moving

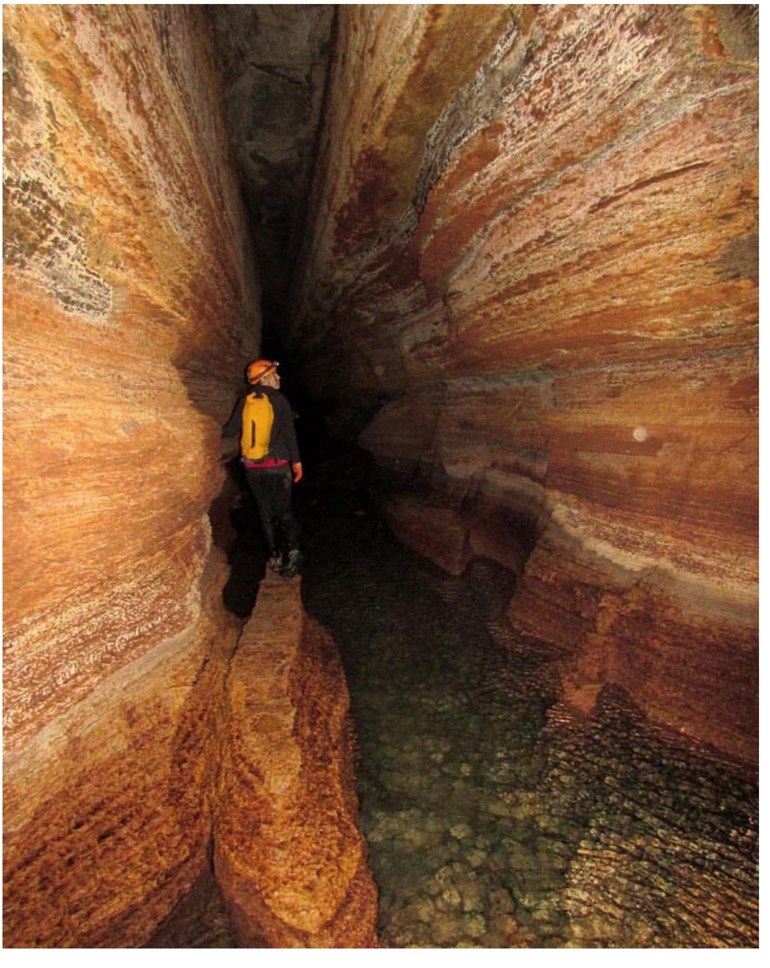

Fig. 12. Photograph of a cave passage showing the linear morphology typical of fracture-controlled speleogenesis (photograph courtesy of Skye Salganek).

the dyes through the system, resulting in different arrival times. Although both dyes were injected during the same day, heterogeneity in snowmelt could have resulted in the delayed movement of uranine through the system.

Although a vertical connection between the C and R aquifers probably still occurs along these fractures, the downward movement of water along these vertical pathways and horizontal flow within the two aquifers are more complex than initially thought. The different flow paths and arrival times at the springs could suggest that the sinkhole where eosin was injected is more closely associated with major conduits, where the dye infiltrated rapidly and then moved quickly through the conduit system to the springs. Conversely, this explanation suggests that the sinkhole into which the uranine was injected is more removed from the conduit system, resulting in slower flow and/or a longer flow path.

Flow paths can vary depending on the intensity of precipitation, the source of water and the antecedent conditions, as has been observed in many other karst systems (Wong *et al.* 2012; Schwartz *et al.* 2013; Reisch & Toran 2014; Parise *et al.* 2015). It is likely that summer precipitation from intense, highly heterogeneous monsoon events results in very different flow patterns from the relatively slow and homogeneous infiltration associated with snowmelt. As a result of the later detection times associated with the uranine dye receptors (May–late July), it is possible that the dye was only partially transported vertically into the subsurface during snowmelt and was not mobilized until monsoonal moisture pushed it through the entire flow system. Conversely, the eosin dye was first detected at receptor sites within a month of injection, indicating that this dye was immediately transported vertically and horizontally through the system with only snowmelt.

Spring hydrograph analysis

Dye trace analyses alone are not sufficient to interpret the complexities of the geology overlying the deep karstic aquifer of the Kaibab Plateau. The spring discharge hydrographs in the deep karst aquifer are affected by the complex structure of the thick, overlying and partially karstified stratigraphy (Fig. 5). Spring hydrograph analysis allows the determination of aquifer water storage and temporal discharge distributions because the discharge can be directly measured in the field (Groves 2007; Fiorillo *et al.* 2012). Karstification leads to a hierarchical arrangement of conduit flow paths that converge and discharge at karst springs (Fiorillo 2014). In karst systems such as the GRCA, and other systems where springs are potable water sources, spring flow monitoring and forecasting are important for ensuring future water supplies (Ford & Williams 2007). Hydrograph analysis at Roaring Springs not only shows a connection between the R aquifer and surface recharge, but also aids in characterizing the vertical and horizontal flow patterns of the hydrogeological system. The discharge response accounts for flow through >1000 m of overlying lithostratigraphic units, including the perched C aquifer. Compared with the shallow karst aquifer system, the spring hydrographs of the deep karstic R aquifer indicate a complex, unknown history of transit time, flow paths and residence times. Analyses of spring hydrographs were used to quantify the dominant flow regimes from both summer monsoon storms and winter snowmelt events, the lag time of the spring response to precipitation and the qualitative amount of recharge contributing to the base flow for different hydrograph peaks. Although other large springs discharge from the R aquifer (e.g. the Vaseys Paradise Spring, Fig. 3), Roaring Springs (Fig. 2) was chosen for analysis because of its importance as the sole water source for visitor, residential and commercial use within the GRCA.

Stage–discharge relationship methods. Previous studies have attempted to collect complete discharge data (Ross 2005; Brown 2011; Schindel 2015), but the sites were inadequate for determining the total flow from Roaring Springs due to non-ideal transducer locations and the lack of high flow discharge measurements during the collection period. For this study, a transducer was relocated to capture all of the flow from Roaring Springs upstream of a distributary system in the cave near the spring's mouth. Because karst spring discharge can vary rapidly compared with other types of springs (Groves 2007), the stage and temperature were recorded at 15 minute intervals with an In-Situ Level TROLL 500 water level data logger (In-Situ, Fort Collins, CO, USA). Ten discrete discharges were measured, including the high flow after peak snowmelt, from November 2015 to August 2016, to create a stage–discharge relationship:

$$\log(Q) = 1.07 \times \log(H) - 0.264 \qquad (2)$$

where Q is the discharge in m^3 s^{-1} and H is the stage in metres. This equation showed a strong correlation between stage and discharge ($r^2 = 0.812$) and a rating curve was used to convert the stage data to continuous discharge values.

Hydrograph analysis methods. The shape of a discharge hydrograph and the timing of response varies with the type of precipitation, the intensity of precipitation, the flow paths and the drainage area. To assess the variability in transit time, groundwater recharge and precipitation response, the hydrographs generated from the transducer data at Roaring

Springs were evaluated for both summer monsoon events and winter snowmelt events. Precipitation was recorded at Bright Angel Ranger Station (COOPID 21001), the closest precipitation gauge to Roaring Springs on the Kaibab Plateau (Fig. 1).

Recession methods. The recession limb of each hydrograph extends from the discharge peak to the beginning of the next rise (Fiorillo 2014). Recession curves were analysed using a modified form of the equation of Maillet (1905), solved for the recession slope:

$$\alpha = \frac{\log\ (Q_n/Q_{n+1})}{0.4343 \times (t_{n+1} -\ t_n)} \tag{3}$$

where α is the recession coefficient in days^{-1}, Q is the discharge in m^3 s^{-1}, t is the time in days, 0.4343 is a constant conversion factor for relating Q and t in their respective units, and n corresponds to the microregime being evaluated. When the recession curve is plotted in semi-logarithmic space as log [Q] v. t, α is the slope of the linear relationship between log [Q] and time. The curve provides a characterization of aquifer drainage. Although Maillet's equation was initially constructed for homogeneous aquifers with high porosity, the equation is useful for comparing more complex karst aquifers (Kresic & Stevanovic 2010). The inverse of the recession coefficient, $1/\alpha$, determines the amount of time it would take for the aquifer to drain if the dominant microregime continued without any other recharge events (Tobin & Schwartz 2016). This value provides a method of comparing microregimes and different recession events.

Comparison of microregimes. Recession curves plotted using equation (3) display multiple straight-line components representing the different levels of aquifer porosity dominating groundwater flow. These different levels of aquifer porosity are referred to as microregimes (Bonacci & Jelin 1988; Kresic & Stevanovic 2010). Multiple microregimes are often observed as a result of the dissolution, structural patterns and conduit development occurring in karst. In the case of Roaring Springs, three microregimes have been identified from the recession curves. The initial steepest slope (α_1 days^{-1}) represents the tertiary porosity or the 'quick flow' through conduits and caves. The intermediate slope (α_2 days^{-1}) indicates the secondary porosity and is probably dominated by water discharging from fractures. The last slope (α_3 days^{-1}) is the flattest and probably represents water discharging slowly from the intergranular (matrix) porosity (Kresic & Stevanovic 2010). The base flow microregime (α_3 days^{-1}) provides a measure of aquifer storage during extended dry periods (Ford & Williams 2007). This is the most stable of the microregimes and is less dependent on surface precipitation patterns. It thus gives the best measure of the characteristics of the matrix porosity (Amit *et al.* 2002).

Regional precipitation patterns can provide long recession periods between precipitation events and flood events at karst springs, thus creating long recession curves for analysis. The Roaring Springs hydrograph data between February 2015 and August 2016 yielded four peaks suitable for recession curve analysis (Fig. 13). Recessions from monsoonal events (mn_1 and mn_2) were analysed and compared with snowmelt recessions (sw_1 and sw_2) (Fig. 13). Although hydrograph responses to the snowmelt events are much more complex, with multiple peaks, the final recession of the snowmelt season provided a method of comparing aquifer microregimes with the summer precipitation.

Storm response timing. The retardation time, or the time from the start of monsoonal precipitation to the spring response, describes the response time of the aquifer to precipitation. An initial increase in spring flow is the result of kinematic waves that pulse through the aquifer, at times 30% faster than the actual water (Ford & Williams 2007). The response of temperature changes at the spring also can be used to more accurately determine the retardation (lag) time of storm water events. The beginning of the decrease in recorded temperature and the bottom or base of the curve (pre-storm arrival) were analysed to determine the monsoonal retardation time rather than the peak discharge. The retardation time from winter snow, which often stays on the ground for days to months before melting and infiltrating the subsurface, is much more complicated and was not analysed.

Recession analysis. Recession curves for the monsoon events mn_1 and mn_2 had different microregime responses from those of the snowmelt events sw_1 and sw_2 (Fig. 14). The snowmelt responses are typified by large complex peaks, whereas the monsoon responses show only one recession slope and have a much lower discharge than the snowmelt responses. The recession curves for the monsoon event mn_1 and the snowmelt events sw_1 and sw_2 have three microregimes, whereas the recession curve for monsoon event mn_2 has only two microregimes. The three recession coefficients for monsoon event mn_1 are steep and about an order of magnitude different (Table 4). Monsoon event mn_2 has only two dominating microregimes, both of which have less steep slopes than mn_1. Monsoon event mn_2 was not as large or as steep as mn_1, which may indicate that the fracture (α_2 days^{-1}) and base flow (α_3 days^{-1}) microregimes are predominant.

The recession curves of the two snowmelt events (sw_1 and sw_2) also differ from each other (Fig. 14).

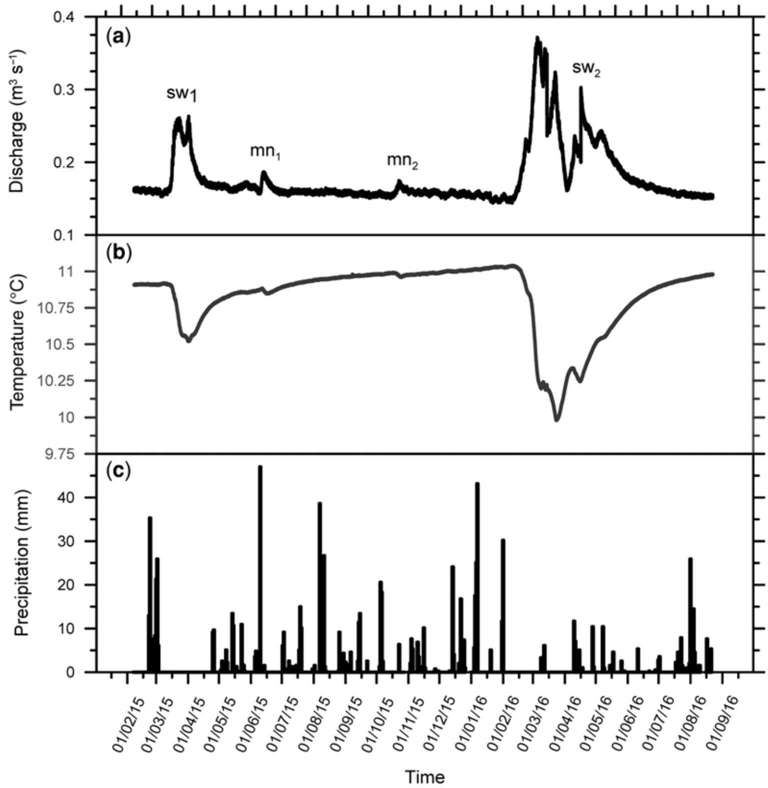

Fig. 13. (**a**) Discharge, (**b**) temperature and (**c**) total daily precipitation data for Roaring Springs cave from 6 February 2015–22 August 2016. sw_1 = early snowmelt recession in April–May 2015, mn_1 = summer monsoonal recession in June–October of 2015, mn_2 = autumn monsoonal recession in October–February 2015–16, sw_2 = snowmelt recession beginning in May 2016 and continuing until the end of data collection (22 August 2016).

Although the transducer was only active from the middle of winter in early February 2015, the response at the end of the 2014–15 winter season is apparent. This season was shorter and drier than the 2015–16 winter season and caused the discharge to appear to be similar to that of monsoon mn_1. The 2015–16 winter season, however, involved substantially more snowfall and subsequent snowmelt. Consequently, all three recession coefficients were much lower for snowmelt event sw_2 (Table 4).

Microregime analysis. The microregimes differed in length and intensity depending on whether the magnitude of various recharge events was sufficient to activate different flow paths in the system (conduit, fracture or intergranular flow). The monsoon recession curves were more influenced by lower magnitude precipitation events than the snowmelt recession curves. For monsoon event mn_1, the amount of time attributed to the conduit (α_1 days^{-1}) and fracture (α_2 days^{-1}) microregimes was relatively short, about six and five days, respectively; monsoon event mn_2 had only two microregimes (α_2 days^{-1}, fracture flow and α_3 days^{-1}, base flow). The fracture flow for monsoon event mn_2 lasted nearly four times as long as the same microregime in monsoon event mn_1 (Table 4). Snowmelt (sw_1), conduit (α_1 days^{-1}) and fracture (α_2 days^{-1}) flow dominated the system for about the first 11 days (2.1 and 8.6 days, respectively) (Fig. 14). For snowmelt (sw_2), however, conduit (α_1 days^{-1}) flow dominated the system for a full 20 days and fracture (α_2 days^{-1}) flow was dominant for 30 days (Table 4).

Storm response timing. The transit time of precipitation from the surface of the plateau to Roaring Springs can only be calculated for discrete monsoon events and not winter snowmelt. A significant rainfall event (mn_1) occurred on 10 June 2015, generating 47 mm of rain (Figs 4 & 13). This rainfall event followed several smaller summer monsoon precipitation events. Roaring Springs began rising one day after the peak and reached a maximum on 13

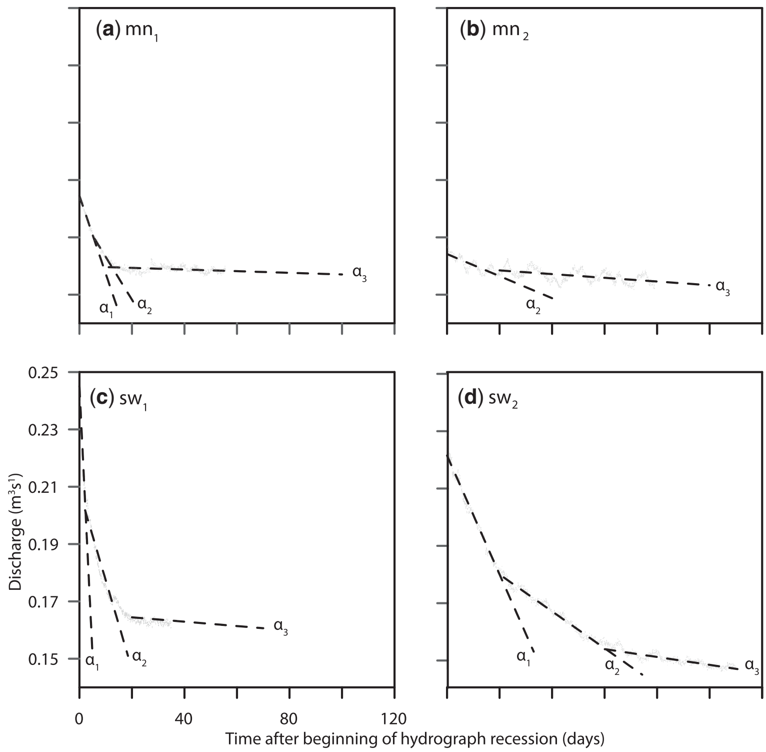

Fig. 14. Recession curves of all four peaks available from the Roaring Springs transducer. (**a**) sw_1 = early snowmelt recession in April–May 2015. (**b**) mn_1 = summer monsoonal recession in June–October 2015. (**c**) mn_2 = autumn monsoonal recession in October–February 2015–16. (**d**) sw_2 = snowmelt recession beginning in May 2016 and continuing until the end of data collection (22 August 2016).

June 2015, three days after the initial rainfall (Figs 4 & 13). The temperature of the spring reached a minimum on 16 June 2015, six days after the major rainfall event (Fig. 4). Monsoon mn_2 discharge and temperature peaks occurred 18 and 20 days after the previous four-day rain event, respectively (Fig. 13). These differences in hydrograph response are represented by the different microregimes

Table 4. *Alpha values (recession coefficients), dates of recessions, microregime duration in days and 1/α for each hydrograph peak and recession for Roaring Springs, 6 February 2015–22 August 2016*

Peak	Event	Recession dates	Alpha value (day^{-1})	Duration of microregime (days)	1/α (days)
mn_1	Monsoon	13 June 2015–8 August 2015	$\alpha_1 = 1.1 \times 10^{-2}$	5.8	97
			$\alpha_2 = 5.9 \times 10^{-3}$	5.3	1.7×10^{2}
			$\alpha_3 = 2.7 \times 10^{-4}$	45	3.7×10^{3}
mn_2	Monsoon	25 October 2015–11 January 2016	$\alpha_2 = 3.0 \times 10^{-3}$	20	3.3×10^{2}
			$\alpha_3 = 3.7 \times 10^{-4}$	59	2.7×10^{3}
sw_1	Snowmelt	2 April 2015–19 May 2015	$\alpha_1 = 8.6 \times 10^{-2}$	2.1	12
			$\alpha_2 = 2.2 \times 10^{-2}$	8.6	45
			$\alpha_3 = 3.3 \times 10^{-4}$	35	5.6×10^{2}
sw_2	Snowmelt	12 May 2016–22 August 2016	$\alpha_1 = 8.1 \times 10^{-3}$	20	1.2×10^{2}
			$\alpha_2 = 3.7 \times 10^{-3}$	30	2.7×10^{2}
			$\alpha_3 = 9.0 \times 10^{-4}$	53	1.1×10^{3}

(Fig. 14). The smaller magnitude precipitation event preceding monsoon event mn_2 was not of sufficient size to create a conduit (α_1 days^{-1}) flow response or was centred far enough away from the spring that the longer flow path resulted in a dampened response (Fig. 14).

Discussion of spring hydrograph analysis. The qualitative assessment of storm responses suggests that only snowmelt events recharge base flow, whereas the flashier monsoon events cause rapid infiltration through the conduit flow paths without recharging matrix storage. The base flow discharge after snowmelt is shown to increase (Fig. 13), whereas after a monsoon event the base flow discharge returns to its original pre-monsoon base flow discharge.

Differences in microregimes between hydrograph recession curves show how the R aquifer responds to different recharge events and can be compared with other karst aquifer systems (Table 5). Karst dolomite springs in the Judean and Galilee mountains of northern Israel (Amit *et al.* 2002), using the approach of Boussinesq (1904), had base flow (α_3 days^{-1}) recession coefficients about an order of magnitude higher than all the Roaring Springs base flow (α_3 days^{-1}) microregime coefficient, except for snowmelt event sw_1. A chalk spring from the same study, however, had a base flow (α_3 days^{-1}) microregime recession coefficient of 6×10^{-4}, which is similar to those for Roaring Springs. Amit *et al.* (2002) concluded that the local lithology has an important role and aquifers with lower permeability have a less steep base flow (α_3 days^{-1}) microregime. The quick flow microregimes of the system, which include both conduit (α_1 days^{-1}) and fracture (α_2 days^{-1}) flow, had variable recession coefficients, with a much higher value for the chalk spring (Amit *et al.* 2002). In the Kaweah river basin (California, USA), karst is present in marble bands (stripe karst) within the granitic to granodioritic host rock of the region (Tobin & Schwartz 2016). Only base flow (α_3 days^{-1}) recession coefficients were included in this study and the results were similar to the Israeli springs reported by Amit *et al.* (2002). The recession curve for the Crnojevića Spring in the Dinaric karst of Montenegro was analysed after the Cetinje polje flooded in 1986 (Bonacci 1993). The geology in this area consists largely of Mesozoic limestones, with some Quaternary dolomite (Bonacci 1993). The average base flow (α_3 days^{-1}) microregime coefficient for the R aquifer via Roaring Springs is 8.4×10^{-4}, which is similar only to the chalk spring from Amit *et al.* (2002). This suggests that the matrix controlling the discharge to Roaring Springs has very low permeability relative to most karst systems (Amit *et al.* 2002). The R aquifer is comparatively deep and overlain with both karst and non-karst features. The relatively flat-lying base flow recession curve could be controlled by either the very low porosity in the R aquifer, the low porosity of the overlying non-karst water-bearing units, such as the Coconino Sandstone, or a combination of water draining from the matrix of both the C and R aquifers.

Variability in precipitation also plays a major part in the variability of the aquifer response (Ford & Williams 2007; Schwartz *et al.* 2013). Precipitation events were highly variable for each hydrograph peak (Fig. 13). The precipitation preceding monsoon event mn_1 was shorter and higher in intensity, with 47 mm of rain in just one day (Fig. 4). Rain preceding monsoon event mn_2 was more temporally distributed, with 58 mm over four days. The location, intensity and antecedent conditions play a major part in defining the amount and type of recharge in the system (Schwartz *et al.* 2013). The perched C aquifer adds to the complications of aquifer response

Table 5. *Summary of seven microregime recession coefficients from previously published work*

Karst region	Geology	Conduit microregime (α_1 day^{-1})	Fracture microregime (α_2 day^{-1})	Intergranular porosity microregime (α_3 day^{-1})	Reference
Judean and Galilee mountains of Israel	Dolomite	2.83×10^{-2}–6.41×10^{-2} (average = 4.48×10^{-2})		3.3×10^{-3}–5.2×10^{-3} (average = 4.2×10^{-3})	Amit *et al.* (2002)
	Chalk	0.1052		6×10^{-4}	
Kaweah River Basin, California, USA	Karstified marble bands within granite to granodiorites	No data	No data	7×10^{-4}–1.27×10^{-2} (average = 5.9×10^{-3})	Tobin & Schwartz (2016)
Crnojevića Spring, Montenegro	Limestone with some dolomite	5.0×10^{-2}	2.7×10^{-2}	1.0×10^{-2}	Bonacci (1993)

with multiple storage types and transport pathways connecting it to the underlying R aquifer (Huntoon 1974).

Conclusions

The interpretations and analyses of the shallow and deep karst aquifers in this study show that the Kaibab Plateau is a highly developed and complex karst region. The surface expression of karst on the Kaibab Plateau resembles internationally recognized karst regions such as the sinkhole plain of south-central Kentucky, USA. The observable increase in sinkhole density in proximity to faults and fractures (or inferred faults and fractures) suggests a strong connection between these structural features and water infiltration into the karst system. Panno *et al.* (2008) have shown a significant relationship between the surface morphology of sinkholes and the underlying conduit system. This relationship in other regions suggests that the surface patterns of the Kaibab Plateau are representative of the shallow conduit system within the karstic portion of the C aquifer. This relationship may indicate that there is significant horizontal flow within the upper C aquifer.

Interpretations of the dye tracer study indicate the prevalence of significant conduit flow and a high level of connectivity between the shallow and deep aquifers. The relatively rapid flow rate of the eosin dye indicates that a large pulse of snowmelt pushed the dye vertically through almost 2000 m of strata in less than five to six weeks, while travelling >40 km horizontally. The rapid subsurface flow is highly indicative of conduit-dominated flow from sinkholes on the surface of the plateau to the springs. This rapid conduit-dominated flow, however, does not determine whether the horizontal flow is predominantly in the shallow C aquifer or the deeper R aquifer. There is a distinct possibility that horizontal flow could be occurring in conduits within either the shallow system, deep system, or both, with vertical flow occurring along fractures and faults in numerous locations.

The locations of detection and slower rate of flow for the uranine dye complicate the interpretation of flow paths. Uranine dye appeared counter-flow to the apparent direction of travel of the eosin dye and took an additional 8–12 weeks to travel through the system and be detected at springs. The apparent difference in flow paths could be due to different vertical flow paths through the system or to a shift in the regional groundwater divide depending on the amount of precipitation and the antecedent conditions. The longer travel time for the uranine dye indicates that the flow paths are either slower because of the conduit morphology or length, or activated by different precipitation regimes from some of the sinkholes on the plateau. The different flow paths are illustrative of the complicated heterogeneity associated with Grand Canyon karst, including vertical flow paths through non-karstic units and other variations between the sinkholes used for the dye injections and their relationship with the underlying conduits.

The possible differences in dye flow paths, arrival times and locations may be seen in the differences in hydrograph responses to snowmelt and monsoonal events. There are significant differences in the responses between the snowmelt and monsoonal storm events. These hydrograph variabilities indicate differences in the dominant flow paths during the recession limb. Snowmelt probably results in recharge and flow through conduits, faults and fractures, and recharge to the intergranular matrix, whereas the monsoonal events show the activation of primarily the conduit/fracture components of the aquifer, not the matrix. Differences in the travel times of these events are probably due to the heterogeneity of rainfall, the configuration of the flow path and the distance from the recharge source to the spring.

Once flow recesses to the base level, the recession coefficients (α mean = 0.00047) are an order of magnitude lower than those measured in other karst systems (i.e. Amit *et al.* 2002; Tobin & Schwartz 2016). The smaller recession coefficients of the Kaibab Plateau demonstrate that the base flow is emerging from matrix storage that has a substantially lower permeability than in most karst systems. This is consistent with the fact that, elsewhere in the Greater Grand Canyon region, the Coconino Sandstone is the significant, but low permeability, water-bearing unit in the C aquifer and releases water from storage that becomes an increasingly more important contributor to the base flow of the R aquifer. The well-indurated limestones that compose the R aquifer have negligible matrix permeability, but dissolution along fractures and bedding planes or partings can account for some of the contribution to base flow.

Our interpretations of the complex interactions of the shallow and deep karst aquifers of the Kaibab Plateau demonstrate how challenging it is to understand the coupled systems. The integration of multiple methods with dye tracers, geospatial analyses of the surface karst and hydrograph analyses allow the verification of aquifer models in a way that cannot be achieved with only one technique. These tools are vital in truly understanding karst aquifers and will allow planning of long-term impacts on water use from potential hazards. Through a combination of reinterpreting old data coupled with new analyses and data, the aquifer systems of the Kaibab Plateau appear to defy previous assumptions of flow path directions and storage patterns and encompass multiple aquifers and lithologies that are crucial in maintaining the flow of springs in the Grand Canyon. Some distinct flow patterns can be linked to major faults, caves and work hypothesized in the 1970s; however, some of those original hypotheses have been revised. Sinkhole characterization, dye trace analysis and hydrograph recession curve analysis provide an initial baseline of understanding of the shallow and deep karstic aquifer systems of the Kaibab Plateau and GRCA and can be used to develop strategies for protecting the Roaring Springs water supply as the sole source of water used in the GRCA. However, a considerable amount of work remains to be done to truly understand the dynamics of groundwater flow and the relationship between the shallow and deep karst aquifers in this region.

This research was conducted under NPS research permit #: GRCA-2016-SCI-0028. Essential funding was provided by the Geological Society of America, the National Park Service's Geoscientists-in-the-Parks Program and the Environmental Stewards Program. The authors thank Peter Huntoon for pre-submission editing and guidance, Lawrence Spangler for his helpful review and an anonymous reviewer.

References

AMIT, H., LYAKHOVSKY, V. *ET AL.* 2002. Interpretation of spring recession curves. *Ground Water*, **40**, 543–551, https://doi.org/10.1111/j.1745-6584.2002.tb02539.x

ANDERSON, M.F. 2000. *Polishing the Jewel: An Administrative History of Grand Canyon National Park*. Grand Canyon Association, Monographs, **11**.

BAKALOWICZ, M. 2005. Karst groundwater: a challenge for new resources. *Hydrogeological Journal*, **13**, 148–160.

BASSO, A., BRUNO, E., PARISE, M. & PEPE, M. 2013. Morphometric analysis of sinkholes in a karst coastal area of southern Apulia (Italy). *Environmental Earth Sciences*, **70**, 2545–2559.

BATZ, N., COLOMBINI, P. *ET AL.* 2016. Groundwater controls on biogeomorphic succession and river channel morphodynamics. *Journal of Geophysical Research: Earth Surface*, **121**, 1763–1785, https://doi.org/10.1002/2016JF004009

BENISCHKE, R., GOLDSCHEIDER, N. & SMART, C. 2007. Tracer techniques. *In*: GOLDSCHEIDER, N. & DREW, D. (eds) *Methods in Karst Hydrogeology*. IAH International Contributions to Hydrogeology, **26**. CRC Press, Boca Raton, FL, 147–170.

BEUS, S.S. 1990*a*. Redwall limestone and surprise canyon formation. *In*: BEUS, S.S. & MORALES, M. (eds) *Grand Canyon Geology*. Oxford University Press, New York, 119–145.

BEUS, S.S. 1990*b*. Temple Butte Formation. *In*: BEUS, S.S. & MORALES, M. (eds) *Grand Canyon Geology*. Oxford University Press, New York, 107–117.

BLAKEY, R.C. 1990. Supai Group and Hermit Formation. *In*: BEUS, S.S. & MORALES, M. (eds) *Grand Canyon Geology*. Oxford University Press, New York, 147–182.

BONACCI, O. 1993. Karst springs hydrographs as indicators of karst aquifers. *Hydrological Sciences Journal*, **38**, 51–62, https://doi.org/10.1080/02626669309492639

BONACCI, O. & JELIN, J. 1988. Identification of a karst hydrological system in the Dinaric karst (Yugoslavia). *Hydrological Sciences Journal*, **33**, 483–497, https://doi.org/10.1080/02626668809491276

BOUSSINESQ, J. 1904. Recherches théoriques sur l'écoulement des nappes d'eau infiltrées dans le sol et sur le debit des sources. *Journal de Mathématiques Pures et Appliquées*, **10**, 5–78.

BRINKMANN, R., PARISE, M. & DYE, D. 2008. Sinkhole distribution in a rapidly developing urban environment: Hillsborough County, Tampa Bay area, Florida. *Engineering Geology*, **99**, 169–184.

BROWN, C.R. 2011. *Physical, geochemical, and isotopic analysis of R-aquifer springs, North Rim, Grand Canyon, Arizona*. Master's thesis, Northern Arizona University.

CAYAN, D.R., DAS, T., PIERCE, D.W., BARNETT, T.P., TYREE, M. & GERSHUNOV, A. 2010. Future dryness in the southwest US and the hydrology of the early 21st century drought. *Proceedings of the National Academy of Sciences, United States of America*, **107**, 21271–21276, https://doi.org/10.1073/pnas.0912391107

CLOW, D.W., SCHROTT, L. *ET AL.* 2003. Ground water occurrence and contributions to streamflow in an alpine catchment, Colorado Front Range. *Groundwater*, **41**, 937–950.

CROSSEY, L.J., FISCHER, T.P. *ET AL.* 2006. Dissected hydrologic system at the Grand Canyon: interaction between deeply derived fluids and plateau aquifer waters in modern springs and travertine. *Geology*, **34**, 25–28, https://doi.org/10.1130/G22057.1

CULVER, D.C. & SKET, B. 2000. Hotspots of subterranean biodiversity in caves and wells. *Journal of Cave and Karst Studies*, **62**, 11–17.

ESRI 2014. *ArcGIS Desktop: Release 10.2*. Environmental Systems Research Institute, Redlands, CA.

FAULKNER, T.L. 2009. The endokarstic erosion of marble in cold climates: Corbel revisited. *Progress in Physical Geography*, **33**, 805–814, https://doi.org/10.1177/0309133309350266

FIORILLO, F. 2014. The recession of spring hydrographs, focused on karst aquifers. *Water Resources Management*, **28**, 1781–1805, https://doi.org/10.1007/s11269-014-0597-z

FIORILLO, F., REVELLINO, P. & VENTAFRIDDA, G. 2012. Karst aquifer draining during dry periods. *Journal of Cave and Karst Studies*, **74**, 148–156, https://doi.org/10.4311/2011JCKS0207

FORD, D. & WILLIAMS, P. 2007. *Karst Hydrogeology and Geomorphology*. Wiley, Chichester.

GOLDSCHEIDER, N., DREW, D. & WORTHINGTON, S. 2007. Introduction. *In*: GOLDSCHEIDER, N. & DREW, D. (eds) *Methods in Karst Hydrogeology*. IAH International Contributions to Hydrogeology, **26**. CRC Press, Boca Raton, FL, 1–8.

GREMAUD, V. & GOLDSCHEIDER, N. 2010. Geometry and drainage of a retreating glacier overlying and recharging a karst aquifer, Tsanfleuron-Sanetsch, Swiss Alps. *Acta Carsologica*, **39**, 289–300.

GROVES, C. 2007. Hydrological methods. *In*: GOLDSCHEIDER, N. & DREW, D. (eds) *Methods in Karst Hydrogeology*. IAH International Contributions to Hydrogeology, **26**. CRC Press, Boca Raton, FL, 45–64.

HAN, G. & LIU, C.Q. 2004. Water geochemistry controlled by carbonate dissolution: a study of river waters draining from karst-dominated terrain, Guizhou Province, China. *Chemical Geology*, **204**, 1–21.

Hart, R.J., Rihs, J. *et al.* 2002. *Assessment of Spring Chemistry Along the South Rim of Grand Canyon in Grand Canyon National Park, Arizona*. US Geological Survey Fact Sheet, **096-02**.

Hereford, R. 2007. *Climate variation at Flagstaff, Arizona – 1950 to 2007*. Open-File Report 2007–1410, US Geological Survey, Reston, VA, 17.

Hill, C.A. & Polyak, V.J. 2010. Karst hydrology of Grand Canyon, Arizona, USA. *Journal of Hydrology*, **390**, 169–181.

Hopkins, R.L. 1990. Kaibab Formation. *In*: Beus, S.S. & Morales, M. (eds) *Grand Canyon Geology*. Oxford University Press, New York, 225–245.

Hua, S., Liang, J. *et al.* 2015. How to manage future groundwater resource of China under climate change and urbanization: an optimal stage investment design from modern portfolio theory. *Water Research*, **85**, 31–37.

Huntoon, P.W. 1970. *The hydro-mechanics of the ground water system in the southern portion of the Kaibab Plateau, Arizona*. PhD thesis, University of Arizona.

Huntoon, P.W. 1974. The post-Paleozoic structural geology of the eastern Grand Canyon, Arizona. *In*: Breed, W.J. & Roast, E.C. (eds) *Geology of the Grand Canyon*. Museum of Northern Arizona and Grand Canyon Natural History Association, Flagstaff, AZ, 82–115.

Huntoon, P.W. 1981. Fault controlled ground-water circulation under the Colorado River, Marble Canyon, Arizona. *Ground Water*, **19**, 20–27, https://doi.org/10.1111/j.1745-6584.1981.tb03433.x

Huntoon, P.W. 2000. Variability of karstic permeability between unconfined and confined aquifers, Grand Canyon region, Arizona. *Environmental & Engineering Geoscience*, **6**, 155–170, https://doi.org/10.2113/gseegeosci.6.2.155

Jemcov, I. 2007. Water supply potential and optimal exploitation capacity of karst aquifer systems. *Environmental Geology*, **51**, 767–773.

Karimi, H., Raeisi, E. & Bakalowicz, M. 2005. Characterising the main karst aquifers of the Alvand Basin, northwest of Zagros, Iran, by a hydrogeochemical approach. *Hydrogeology Journal*, **13**, 787–799.

Kresic, N. & Stevanovic, Z. 2010. *Groundwater Hydrology of Springs: Engineering, Theory, Management, and Sustainability*. Butterworth-Heinemann, Amsterdam.

Lauber, U., Ufrecht, W. & Goldscheider, N. 2014. Spatially resolved information on karst conduit flow from in-cave dye tracing. *Hydrology and Earth System Sciences*, **18**, 435–445.

Liu, F., Parmenter, R. *et al.* 2008. Seasonal and interannual variation of streamflow pathways and biogeochemical implications in semi-arid, forested catchments in Valles Caldera, New Mexico. *Ecohydrology*, **1**, 239–252.

Liu, F., Hunsaker, C. & Bales, R. 2012. Controls of streamflow generation in small catchments across the snow–rain transition in the southern Sierra Nevada, California. *Hydrological Processes*, **27**, 1959–1972, https://doi.org/10.1002/hyp.9304

Maillet, E. 1905. *Essai d'hydraulique souterraine et fluviale*. Hermann, Paris.

Middleton, L.T. & Elliot, D.K. 1990. Tonto Group. *In*: Beus, S.S. & Morales, M. (eds) *Grand Canyon Geology*. Oxford University Press, New York, 83–106.

Mueller, J.M., Lima, R.E. & Springer, A.E. 2017. Can environmental attributes influence protected area designation? A case study valuing preferences for springs in Grand Canyon National Park. *Land Use Policy*, **63**, 196–205, https://doi.org/10.1016/j.landusepol.2017.01.029

National Oceanic and Atmospheric Administration 2013. Bright Angel Ranger Station COOPID 21001, data for the period 1948–2013, www.ncdc.noaa.gov/cdo-web/datasets/GHCND/stations/GHCND:USC00021001/detail

Oraseanu, I. & Mather, J. 2000. Karst hydrogeology and origin of thermal waters in the Codru Moma. *Hydrogeology Journal*, **8**, 379–389, https://doi.org/10.1007/s100400000080

Panno, S.V., Angel, J.C., Nelson, D.O., Weibel, C.P., Luman, D.E. & Devera, J.A. 2008. *Sinkhole Distribution and Density of Renault Quadrangle, Monroe County, Illinois*. Illinois State Geological Survey, Champaign, IL.

Panno, S.V., Kelly, W.R., Angel, J.C. & Luman, D.E. 2013. Hydrogeologic and topographic controls on evolution of karst features in Illinois' sinkhole plain. *Carbonates and Evaporites*, **28**, 13–21, https://doi.org/10.1007/s13146-013-0157-2

Parise, M., Ravbar, N., Živanovic, V., Mikszewski, A., Kresic, N., Mádl-Szőnyi, J. & Kukuric, N. 2015. Hazards in karst and managing water resources quality. *In*: Stevanovic, Z. (ed.) *Karst Aquifers – Characterization and Engineering*. Professional Practice in Earth Sciences. Springer, Berlin, 601–687, https://doi.org/10.1007/978-3-319-12850-4_17

Perrin, J., Jeannin, P.-Y. & Zwahlen, F. 2003. Epikarst storage in a karst aquifer: a conceptual model based on isotopic data, Milandre test site, Switzerland. *Journal of Hydrology*, **279**, 106–124, https://doi.org/10.1016/S0022-1694(03)00171-9

Python Software Foundation 2016. Python Programming Language, Version 2.7.12, release date 2016, www.python.org

Reisch, C.E. & Toran, L. 2014. Characterizing snowmelt anomalies in hydrochemographs of a karst spring, Cumberland Valley, Pennsylvania (USA): evidence for multiple recharge pathways. *Environmental Earth Sciences*, **72**, 47–58.

Ross, L.E.V. 2005. *Interpretive three-dimensional numerical groundwater flow modeling, Roaring Springs, Grand Canyon, Arizona*. Master's thesis, Northern Arizona University.

Salcedo-Sanchez, E.R., Esteller, M.V. *et al.* 2013. Groundwater optimization model for sustainable management of the Valley of Puebla aquifer, Mexico. *Environmental Earth Sciences*, **70**, 337–351.

Scanlon, B.R., Mace, R.E. *et al.* 2003. Can we simulate regional groundwater flow in a karst system using equivalent porous media models? Case study, Barton Springs, Edwards aquifer, USA. *Journal of Hydrology*, **276**, 137–158, https://doi.org/10.1016/S0022-1694(03)00064-7

Schindel, G.M. 2015. *Determining groundwater residence times of the Kaibab Plateau, R-aquifer using* *temperature, Grand Canyon National Park, Arizona*. Master's thesis, Northern Arizona University.

SCHINDEL, G.M., JOHNSON, S., VENI, G., SCHNITZ, L. & SHADE, B.L. 2007. *Tracer Test Work Plan Kinney and Uvalde Counties*. Edwards Aquifer Authority, San Antonio, TX.

SCHWARTZ, B.F., SCHWINNING, S. *ET AL*. 2013. Using hydrogeochemical and ecohydrologic responses to understand epikarst process in semi-arid environments, Edwards Plateau, Texas, USA. *Acta Carsologica*, **42**, 315, https://doi.org/10.3986/ac.v42i2-3.670

SHEPPARD, A.C., COMRIE, G.D. *ET AL*. 2002. The climate of the US Southwest. *Climate Research*, **21**, 219–238.

SPRINGER, A.E. & STEVENS, L.E. 2009. Spheres of discharge of springs. *Hydrogeology Journal*, **17**, 83–93, https://doi.org/10.1007/s10040-008-0341-y

SZOCS, T., TÓTH, G. *ET AL*. 2015. Long-term impact of transboundary cooperation on groundwater management. *European Geologist*, **40**, 29–33, http://eurogeologists.eu/wp-content/uploads/2015/11/EGJ40_final_LR.pdf

TOBIN, B.W. & SCHWARTZ, B.F. 2012. Quantifying concentrated and diffuse recharge in two marble karst aquifers: Big Spring and Tufa Spring, Sequoia and Kings Canyon National Parks, California, USA. *Journal of Cave and Karst Studies*, **74**, 186–196.

TOBIN, B.W. & SCHWARTZ, B.F. 2016. Using periodic hydrologic and geochemical sampling with limited continuous monitoring to characterize remote karst aquifers in the Kaweah River Basin, California, USA. *Hydrological Processes*, **30**, 3361–3372.

TROESTER, J.W., WHITE, E.L. & WHITE, W.B. 1984. A comparison of sinkhole depth frequency distributions in temperate and tropical karst regions. *In*: BECK, B.F. (ed.) *Sinkholes: their Geology, Engineering, and Environmental Impact*. A.A. Balkema, Rotterdam, 65–73.

WEARY, D.J. & DOCTOR, D.H. 2014. *Karst in the United States: a Digital Map Compilation and Database*. US Geological Survey Open-File Report **2014–1156**, https://doi.org/10.3133/ofr20141156

WHITE, W.B. 1988. *Geomorphology and Hydrology of Karst Terrains*. 1st edn. Oxford University Press, Oxford.

WONG, C.I., MAHLER, B.J., MUSGROVE, M. & BANNER, J.L. 2012. Changes in sources and storage in a karst aquifer during a transition from drought to wet conditions. *Journal of Hydrology*, **468**, 159–172.

WORTHINGTON, S.R.H. & SMART, C.C. 2003. Empirical determination of tracer mass for sink to spring tests in karst. *In*: BECK, B.F. (ed.) *Sinkholes and the Engineering and Environmental Impacts of Karst*. Geotechnical Special Publication **122**. American Society of Civil Engineers, 287–298.